26

Vision-Based Haptic Feedback with Physically-Based Model for Telemanipulation

Jungsik Kim[1] and Jung Kim[1]
[1]*Korea Advanced Institute of Science and Technology (KAIST)*
South Korea

1. Introduction

Haptic feedback offers the potential to increase the quality and capability of human-machine interactions as well as the ability to skillfully manipulate objects by exploiting the sense of touch (Lin & Salisbury, 2004). Previous studies on haptic feedback systems typically dealt with virtual reality (VR)-based simulations, and telemanipulation systems. VR-based simulation systems used haptic information for various applications such as gaming (Morris, 2004), surgical simulations (Basdogan et al., 2004), or molecular simulations (Ferreira, 2006) in order to provide realistic virtual experiences along with sound and graphic rendering. In telemanipulation, haptic feedback has been studied in the fields of robotic guidance and obstacle avoidance (Hassanzadeh et al., 2005), robotic surgery (Mayer et al., 2007; Wagner et al., 2007) and micro/nano manipulation (Sitti & Hashimoto, 2003, Ammi et al., 2006). According to these studies, the feedback of haptic information to an operator can improve performance and provide telepresence. For example, in nano- or bio-manipulation applications, where the operator manipulates a micro-scale object with limited two-dimensional vision feedback through a microscope, haptic assistance can be used to provide the depth information, generate virtual fixtures or guides and thus improve the operator manipulation final quality (e.g., operation time and efficiency).

The goal of telemanipulation is to create a human operator interaction with a remote environment as closely as possible. Such a goal can be realized by (i) obtaining the available information of the slave site, such as the geometry, kinematic information, and material properties; (ii) applying this information to a user with high-fidelity master devices; and (iii) efficiently conveying the user response to the slave environment through actuating systems. Although many studies on the technical issues encountered in telemanipulation have been carried out, sensing the force information and its reflection to a user still constitutes a challenging issue because of problems associated with sensor design and force rendering.

Sensing the force information of a slave environment is a prerequisite in order to display a user force feedback during manipulation tasks. For example, the realization of a force feedback in telemanipulation has mainly been done thus far by integrating force sensors into a slave site to measure reaction forces between a slave robot and the environment. The

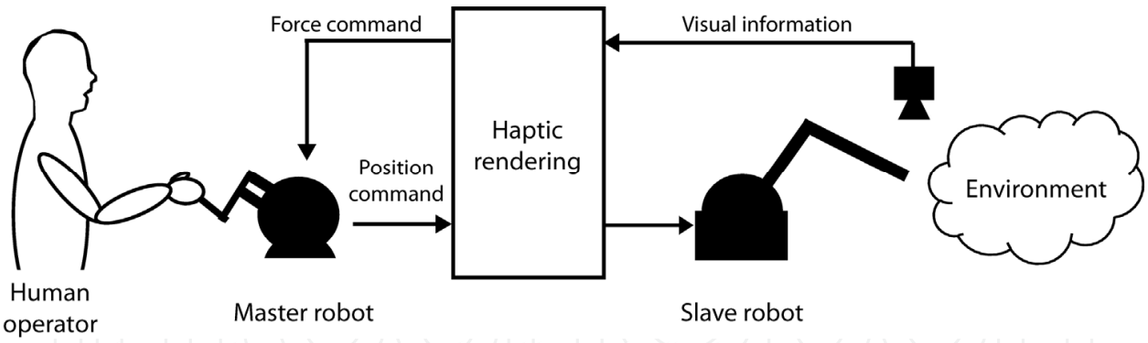

Fig. 1. Telemanipulation with vision-based haptic feedback

measured force signals are then filtered to guarantee the stability of the haptic device and offer an improved quality of the force feedback. The force sensor, however, has a low signal-to-noise ratio (SNR) for force feedback and can be damaged through physical contact with the environment or by exposure to biological and chemical materials. Although the use of a strain-gauge sensor or a commercial six-axes force/torque sensor in teleoperated robotic surgery has been examined (Mayer et al., 2007; Wagner et al., 2007), current commercial surgery robots hardly provide an adequate haptic feedback due to safety and effectiveness issues, partially associated with the reliability of the force sensor in a noisy environment. Very-small-scale force sensing for micromanipulation is more difficult because of the design of small force sensors that needs to meet challenging requirements for such applications, including micro-sensing for multiple degrees of freedom (DOF) with high resolution and accuracy while maintaining a high SNR. In addition, sufficient reliability and repeatability of the force sensor must be preserved. In particular, micro-scale measurements for biomanipulation are subject to severe disturbances due to the liquid surface tension (e.g., when cells are in a medium) and adhesion forces (Lu et al., 2006; Gauthier & Nourine, 2007). Therefore, new methods capable of avoiding the use of the force sensors have recently become very prevalent.

This chapter presents a new method for rendering the interaction forces of a slave environment based on visual information rather than on direct force measurements using a force sensor (Fig. 1). The visual information measured from optical devices is transformed into haptic information by modeling the slave environment. The interaction forces are rendered from this environment using a mechanical model representing the relationship between the object deformation and the applied forces. Therefore, it is not necessary to use force sensors. Originally, the term "haptic rendering" was defined as the process of computing and generating forces in response to a user interaction with virtual objects (Salisbury et al., 1995), including collision detection, force response, and control algorithms (Salisbury et al., 2004). The proposed algorithm also incorporates these components in order to compute and generate forces due to the user interaction with the visually modeled slave environment.

The interaction force prediction algorithm is investigated using image processing and physically-based modeling techniques. The geometry (boundary) information of a deformable object is obtained from images of the slave site in pre-process, and the kinematic information of a slave tool tip can be obtained using a fast image processing algorithm for the input of the physically-based model to estimate the interaction forces. In this Chapter, the boundary element method (BEM) is used as a physically-based modeling technique for

the modeling while a priori knowledge of the material properties is assumed. During the interactions, the boundary conditions are updated using a real-time motion analysis of the slave environment. The interaction forces are then calculated based on the model, and are then conveyed to the user through a haptic device. The proposed algorithm only requires the material properties and the object edge information. Thus, this algorithm is robust to topological changes of the model network. In addition, measuring the deformation of an entire object body and applying it to the model as nodal displacements can be a very time-consuming work. Therefore the position update of a slave robot (tool tip) is used to recover the forces, similarly to the haptic interaction point (HIP) in VR applications (Massie & Salisbury, 1994). Moreover, the proposed system addresses the force sensing issues in both micro- and macro-scales so that a very small- or very large-scale slave environment can be rendered using the proposed algorithm.

This chapter is organized as follows: Section 2 presents the previous work related to vision-based force estimation methods. Section 3 provides an overview of the proposed haptic rendering algorithm, which is based on image processing and physically-based modeling techniques. In order to demonstrate the effectiveness of the proposed method, macro- and micro-scale telemanipulation systems were developed. In Section 4, the experimental results of the developed telemanipulation systems are presented. Finally, conclusions and suggestions with regard to future work are given in Section 5.

2. Previous Work

A large number of computer vision and image processing techniques have been investigated with regard to the object recognition and tracking (Ogawa et al., 2005), the characterization of material properties (Tsap et al., 2000; Liu et al., 2007a), the collision detection (Wang et al., 2007), and the modeling of deformable objects (Metaxas & Kakadiaris, 2002). In this context, the force estimation from visual information has also received much attention. Forces are usually computed based on the geometric information of an object (or a manipulator) for the known input displacements, for which the measured geometrical information is applied to a force estimation algorithm. For instance, Wang et al. (2001) computed the deformation gradients of elastic objects from images and estimated the external forces using the stress-strain relationships. Luo and Nelson (2001) presented a method fusing force and vision feedback for a deformable object manipulation, in which the measured deformation was applied to a finite element (FE) model to obtain the force estimates. Greminger and Nelson (2004) showed a force measurement through the boundary displacements of elastic objects using a Dirichlet-to-Neumann map. Nelson et al. (2005) measured the applied forces for biological cells with a point-load model for cell deformation. DiMaio and Salcudean (2003) measured the tissue phantom deformation to estimate the applied force distribution during the insertion of a needle. Anis et al. (2006) used the force-displacement relationship of a micro-gripper in a microassembly process. Liu et al. (2007b) measured the contact forces of a biological single-cell using the deflection of a polydimethylsiloxane (PDMS) post in a cell holding device.

A few researchers have studied the real-time force estimation algorithms for haptic rendering based on visual information. Owaki et al. (1999) introduced a concept in which the visual data of real objects were used as haptic data to simulate the virtual touching of an object, but not for telemanipulation tasks. They used a high-speed active-vision system

allowing to obtain visual data at 200 Hz. Ammi et al. (2006) used microscopic images to provide haptic feedback in a cell injection system. A cell nonlinear mass-spring model was used to compute the interaction forces for haptic rendering. However, mass-spring models offer limited accuracy (Kerdok et al., 2003). Other significant disadvantages of their method include its weak connection to biomechanics. For example, there was no mechanically relevant relationship between the model parameters and the object material properties. Moreover, the parameters were calculated from off-line finite element method (FEM) simulations; this required extra FE modeling efforts and the results were influenced by the network topology. Kennedy and Desai (2005) proposed a vision-based haptic feedback system in the case of robot-assisted surgery. A rubber membrane was modeled using a FE model, and a grid located on the rubber membrane was visually tracked in order to measure its displacement. The FE model then reflected the interaction forces using the displacement values as boundary conditions. With this method, however, it was necessary to stamp a grid pattern on the object to generate the internal meshes and track each node for the FE model, which made this method inconvenient and impractical for biological- and micro-scale objects. In addition, real-time solution of FEM is usually not feasible (Delingette, 1998).
In conclusion, the mass-spring system and FEM model in the aforementioned studies present severe shortcomings, often requiring additional efforts. FEM models were not efficient enough to be used in real-time applications. Finally, in many of the previous systems, the FEM required a controlled slave environment to model the membrane. The mass-spring model was usually non-realistic and highly-sensitive to the tuning of the model, such as in the spring constant of the mesh, through additional experiments. To circumvent the issues related to the use of FEM and mass-spring models, the present paper uses BEM as an alternative approach to estimate the forces required for the haptic feedback. BEM is a numerical solution technique to solve the differential equations representing an object model that computes the unknowns on the model boundary instead of on its entire body. The proposed method uses the object edge information and known material properties, which make it highly adaptive to the network topology changes by reducing the amount of additional effort required in previous systems.

3. Vision-Based Haptic Interaction Method

3.1 Overview

Fig. 2 represents the coordinates of the developed system. A master interface has a master space with frame $\mathbf{\Phi}$ in which the position of the haptic stylus is given by the three-dimensional (3D) vector ${}^{\Phi}\mathbf{p}$. The physical interactions between a manipulator and a deformable object are introduced in the slave space $\boldsymbol{\varphi}$. The shape of an object can be expressed by ${}^{\varphi}\mathbf{q}$ and the position of the manipulator ${}^{\varphi}\mathbf{p}$ is related to ${}^{\Phi}\mathbf{p}$ by the transform $\mathbf{T}^{P}$. The interactions in the slave space are mapped to the image space $\mathbf{I}$ to measure the position ${}^{\varphi}\mathbf{p}$ and ${}^{\varphi}\mathbf{q}$ and to estimate the interaction force ${}^{\varphi}\mathbf{F}=f({}^{\varphi}\mathbf{q}, {}^{\varphi}\mathbf{p})$, where $f(\cdot)$ represents the continuum mechanics method. The interaction force ${}^{\varphi}\mathbf{F}$ is then transformed into ${}^{\Phi}\mathbf{F} = \mathbf{T}^{F} \cdot {}^{\varphi}\mathbf{F}$ using the transform $\mathbf{T}^{F}$. The transforms $\mathbf{T}^{P}$ and $\mathbf{T}^{F}$ contain scaling factors between the master and slave spaces. If a position scaling factor in $\mathbf{T}^{P}$ is set to scale down (or up), the forces are scaled up (or down) by a force scaling factor in $\mathbf{T}^{F}$.

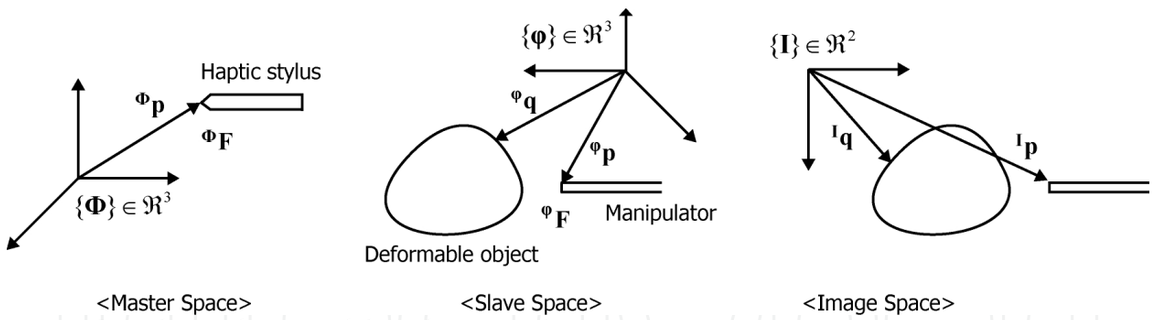

Fig. 2. Coordinate frames of the telemanipulation system

The algorithm consists of two parts (Fig. 3): the construction of a deformable object model (preprocess) and the interaction force update for each frame (run-time process). In the preprocess phase, the edge information of the object is obtained using image processing techniques, and a boundary mesh is constructed based on the edge information. The boundary element (BE) model is then created with the object mesh and known material properties. Using this model, the system of equations is built and pre-computed; it is used for a fast update of the system matrix in the run-time process.

In the run-time phase, collision detection and force computations are performed at a rate of 1 kHz. When a user interacts with a deformable object, the displacement at the contact point is applied to the model as a boundary condition. The boundary contact force is then computed using the BEM. If the displacement magnitude or the contact point changes, new force values can be obtained by updating the boundary conditions using real-time image processing and by applying them to the pre-computed system matrix in the preprocess phase.

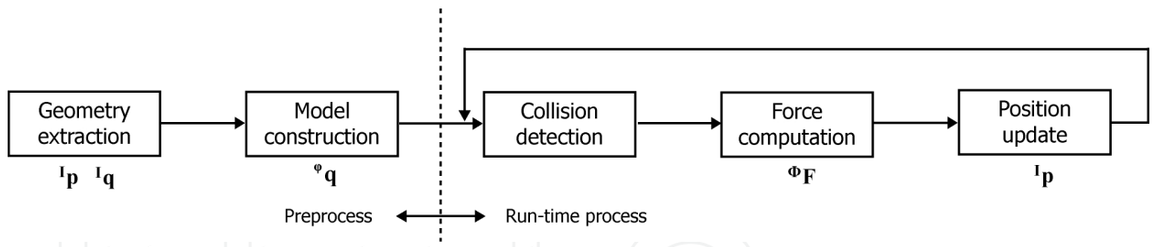

Fig. 3. The force prediction algorithm pipeline

The key parts of the algorithm consist of the geometry extraction from images, the object modeling and the real-time computation of the interaction forces. The remainder of this Section concretely explains each part of the algorithm.

3.2 Geometry Extraction

Fast and accurate motion tracking and edge detection techniques are important for modeling a deformable object. The edge ($^{\mathrm{I}}\mathbf{q}$) of the object along with the tool tip position ($^{\mathrm{I}}\mathbf{p}$) of a slave-manipulator is extracted and tracked using the following methods.

A template matching is used to track the tool tip position ($^{\mathrm{I}}\mathbf{p}$), which is a process that determines the location of a template by measuring the degree of similarity between an image and the template. Although there are several methods that can measure the degree of

similarity, such as the summation of the squared difference (SSD), a normalized cross-correlation coefficient was implemented to reduce the degree of sensitivity to contrast changes in the template and in the video image (Aggarwal et al., 1981). The correlation between the pixel of the template (w × h) and every pixel in the entire image is given by

$$\tilde{C}({}^{I}x,{}^{I}y)=\frac{\sum_{{}^{I}y'}^{h-1}\sum_{{}^{I}x'}^{w-1}\tilde{T}({}^{I}x',{}^{I}y')\tilde{I}({}^{I}x+{}^{I}x',{}^{I}y+{}^{I}y')}{\left(\sum_{{}^{I}y'}^{h-1}\sum_{{}^{I}x'}^{w-1}\tilde{T}({}^{I}x',{}^{I}y')^{2}\sum_{{}^{I}y'}^{h-1}\sum_{{}^{I}x'}^{w-1}\tilde{I}({}^{I}x+{}^{I}x',{}^{I}y+{}^{I}y')^{2}\right)^{1/2}} \tag{1}$$

where $\tilde{I}({}^{I}x+{}^{I}x',{}^{I}y+{}^{I}y')=I({}^{I}x+{}^{I}x',{}^{I}y+{}^{I}y')-\bar{I}({}^{I}x,{}^{I}y)$, $\tilde{T}({}^{I}x',{}^{I}y')=T({}^{I}x',{}^{I}y')-\bar{T}$. $I({}^{I}x,{}^{I}y)$ and $T({}^{I}x,{}^{I}y)$ are the corresponding values at location $({}^{I}x,{}^{I}y)$ of the image and template pixels, respectively. $\bar{I}({}^{I}x,{}^{I}y)$ and $\bar{T}$ are the average pixel value in the template and the average pixel value in the image under the template window, respectively. In order to reduce the computational load of the pixel-by-pixel operation (Equation 1), a moving region-of-interest (ROI) is adopted. As the movement of the tool tip is very small in the sequential frames, the ROI is determined around the identified position via a template matching. The template matching is then performed in the ROI to obtain the new position.
To represent the geometry ($^{\varphi}\mathbf{q}$) of a deformable object, the two-dimensional object boundary ($^{I}\mathbf{q}$) is extracted using the active contour model (snake) developed by Kass et al. (1988). The contour with a set of control points is initially manually placed near the edge of interest. The energy function defined surrounding each control point is then computed, and the contour is drawn to the edge of the image where the energy has a local minimum. In this paper, a fast greedy algorithm (Williams & Shah, 1992) for energy minimization is used and the energy function E_{snake} is defined by

$$E_{snake} = \int(\alpha(s)\cdot E_{cont} + \beta(s)\cdot E_{curv} + \gamma(s)\cdot E_{image})ds \tag{2}$$

Here, s is the arc-length along the snakes contour taken as a parameter. The continuity energy E_{cont} minimizes the distance between control points and prevents all control points from moving toward the previous control point. E_{curv} represents the curvature energy and it is responsible for the curvature of the contour corner. The image energy E_{image} indicates the normalized edge strength. The values of α, β and γ determine the factors of each energy term. The edge of the object is finally represented by the positions of the control points which are used to mesh the boundary of the object for the BE model.

3.3 Continuum Mechanics Model

For realistic and plausible force estimation, the continuum mechanics modeling of a deformable object has been widely studied and developed in haptic applications (Meier et al., 2005). In continuum mechanics, differential equations for the stress- or strain-equilibrium have to be solved and numerical methods such as FEM and BEM are usually used with a discretization of the object into a number of elements.

The BEM directly uses mechanical parameters and handles various interactions between the tools and the objects. Due to its physically-based nature and computational advantages over the FEM, it has been used in computer animation and haptic applications. James and Pai (2003) successfully applied BEM to the simulation of a deformable object with haptic feedback. The reaction force and deformation were computed based on pre-computed reference boundary value problems known as Green's functions (GFs) and a capacitance matrix algorithm (CMA).

In this work, the BE model of a deformable object was built using the extracted object edge information using the control points of an active contour model and the related material properties (Young's modulus E and Poisson's ratio ν). The boundary of the object was discretized into N elements. The points representing the unknown values, tractions (forces per unit area) and displacements are defined as nodes. In the present study, we have selected constant elements for simplicity, namely the nodes are assumed to be in the middle of each element and the unknowns have a constant value over each element. The resulting system of equations is given by Equation 3 (Kim et al., 2009).

$$\mathbf{HP} = \mathbf{GV} \tag{3}$$

Here, the $\mathbf{H}(E, \nu, \mathbf{q})$ and $\mathbf{G}(E, \nu, \mathbf{q})$ matrices are 2N × 2N dense matrices in the case of 2D problems. $\mathbf{P}$ and $\mathbf{V}$ are the displacement and traction vectors, respectively. The boundary conditions, displacements or tractions, are applied at each node to solve these algebraic equations. When the displacement value is given on a node, the traction value can be obtained, and vice versa. Equation 3 can be rearranged as

$$\mathbf{AY} + \bar{\mathbf{A}}\bar{\mathbf{Y}} = \mathbf{0} \rightarrow \mathbf{Y} = \mathbf{A}^{-1}(-\bar{\mathbf{A}}\bar{\mathbf{Y}}), \tag{4}$$

where $\mathbf{Y}$ is the unknown vector consisting of unknown boundary nodal values, and $\bar{\mathbf{Y}}$ represents the known boundary conditions. $\mathbf{A}$ and $\bar{\mathbf{A}}$ consist of the columns of the $\mathbf{H}$ and $\mathbf{G}$ matrices according to the indices of $\mathbf{Y}$ and $\bar{\mathbf{Y}}$, respectively. $\mathbf{Y}$ can be obtained by solving Equation 4.

When an object is deformed, the boundary conditions at the collision nodes change. Therefore, Equations 3 and 4 must be rewritten to take the new boundary conditions into account and they must be solved in real-time.

3.4 Real-Time Force Computation

For a real-time and realistic haptic interaction, it is necessary to provide a haptic feedback with updating rates greater than 500 Hz (Chen & Marcus, 1998). In other words, the interaction forces must be computed within 2 msec. In order to solve the linear matrix system of Equation 4 in real-time, a CMA is used (James & Pai, 2003). If the S boundary conditions change for the linear elastic model, the $\mathbf{A}$ matrix for a new set of boundary conditions can be related to the pre-computed $\mathbf{A}_0$ matrix by swapping simple S block columns. Using the Sherman-Morrison-Woodbury formula, the relationship between $\mathbf{A}$ and $\mathbf{A}_0$ can be obtained as follows:

$$\mathbf{A}^{-1} = \mathbf{A}_0^{-1} - \mathbf{A}_0^{-1}(\bar{\mathbf{A}}_0 - \mathbf{A}_0)\mathbf{I}_S\mathbf{C}^{-1}\mathbf{I}_S^T\mathbf{Y}_0 \tag{5}$$

Equation 4 can be then represented by

$$\mathbf{Y} = \mathbf{A}^{-1}(-\bar{\mathbf{A}}\bar{\mathbf{Y}}) = \mathbf{Y}_0 + (\mathbf{I}_S + \Xi\mathbf{I}_S)\mathbf{C}^{-1}\mathbf{I}_S^T\mathbf{Y}_0$$

$$\begin{aligned} \mathbf{C} &= -\mathbf{I}_S^T\Xi\mathbf{I}_S \\ \Xi &= -\mathbf{A}^{-1}\bar{\mathbf{A}} \\ \mathbf{Y}_0 &= \left[\Xi(\mathbf{I} - \mathbf{I}_S\mathbf{I}_S^T) - \mathbf{I}_S\mathbf{I}_S^T\right]\bar{\mathbf{Y}} \end{aligned} \tag{6}$$

Here, $\mathbf{I}_S$ is an 2N × 2S submatrix of the identity matrix, $\mathbf{C}$ is known as the capacitance matrix (2S × 2S) and $\mathbf{Y}_0$ is computed using Equation 4. The GFs Ξ is computed for a predefined set of boundary conditions in the preprocess phase. Equation 6, known as the capacitance matrix formulae, can then be implemented to reduce the amount of re-computation. The solution $\mathbf{Y}$ for the tractions and displacements over the entire boundary can be obtained by computing the inverse of the smaller capacitance matrix. For example, in the case of a point contact, S =1, only a 2 × 2 matrix inversion is required.

It is not necessary to compute the global deformation because the visual feedback is provided through real-time video images rather than using computer-generated graphic images. Given the nonzero displacement boundary conditions at the contact S nodes, the resulting contact force can be computed by

$${}^{\Phi}\mathbf{F} = \alpha_E\mathbf{V}_S = \alpha_E\mathbf{I}_S^T\mathbf{Y} = -\alpha_E\mathbf{C}^{-1}\mathbf{I}_S^T\bar{\mathbf{Y}} = -\alpha_E\mathbf{C}^{-1}\bar{\mathbf{Y}}_S \tag{7}$$

Here, α_E is the effective area. It consists of the nodal area and a scaling factor for different-scale manipulation tasks in order to magnify (or reduce) the contact force while providing a haptic feedback to the user.

Although the contact forces are rapidly computed using locally updated boundary conditions, the forces are obtained at a visual update rate (of approximately 60 Hz) because of the boundary conditions that are updated from the images. It is insufficient to achieve a good fidelity haptic feedback. Therefore, a force interpolation method (Zhuang & Canny, 2000) is used to derive the forces at high rates (1 kHz).

3.5 Collision Detection

The collision detection is achieved utilizing hierarchical bounding boxes and a neighborhood watch algorithm (Ho et al., 1999). The BE model is hierarchically represented as oriented bounding box trees and stored in a preprocess phase. If a line segment between the previous and current tool tip positions is inside the bounding box, potential collisions are sequentially checked along the tree. When the last bounding box for the line element collides with the line segment, the ideal haptic interface point is constrained at the collision node. The distance between the tool tip and the collision node is used as the displacement boundary condition of the node. During interactions, the collision nodes are rapidly

updated using a neighborhood watch algorithm, which is based on a predefined linkage between the nodes.

4. Case Studies and Results

The developed algorithm was evaluated for the manipulation of elastic materials with different scales. Two experiments were conducted to demonstrate the effectiveness of the algorithm in macro- and micro-telemanipulation tasks. In both systems, the deformation of the objects and the motion of a slave robot were captured by a CCD camera (SVS340MUCP, SVS-Vistek, Seefeld, Germany with 640 × 480 pixels resolution and maximum of 250 fps) and the images were transmitted to a computer (Pentium-IV 2.40 GHz). The 2D geometry information can be known through image processing techniques using OpenCV. A commercial haptic device (SensAble Technologies, PHANToM OmniTM, USA) was used for force feedback and a priori knowledge of the material properties was obtained through the experiment and from the literature. The behavior of the model during manipulation was compared with that from a real deformable object. The overall system block diagram is shown in Fig. 4.

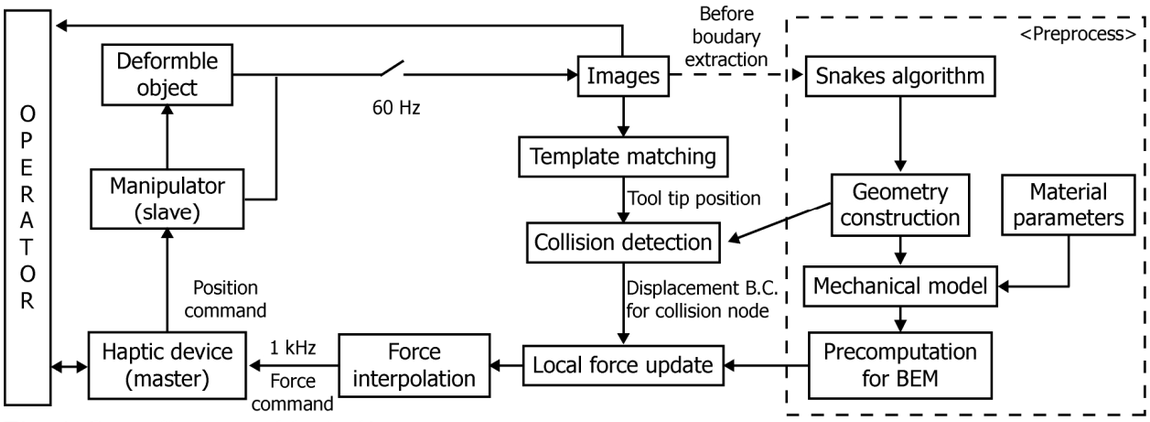

Fig. 4. Overall system block diagram

4.1 Experiment 1: Macro-Scale Telemanipulation System

The macro-scale manipulation system consists of an inanimate deformable object and a planar manipulator with an indenter tip as a slave robot. Fig. 5 shows the setup for the experimental platform. A 3 DOF planar manipulator (500 mm × 500 mm) performs indentation tasks on a rectangular-shaped object made from silicone gel (88 mm × 88 mm × 9 mm, GE, TSE3062, USA). The Young's modulus of the silicone block is 127 kPa (Kim et al., 2008; Kim et al., 2009). The images obtained using a CCD camera have a size of 640×480 pixels and a resolution of 0.35 mm/pixel. In addition, the indentation force is measured using a one-axis force sensor (Senstech, SUMMA-5K, Korea) with a resolution of 50 mN. The force sensor is used to validate the estimated force from visual information.

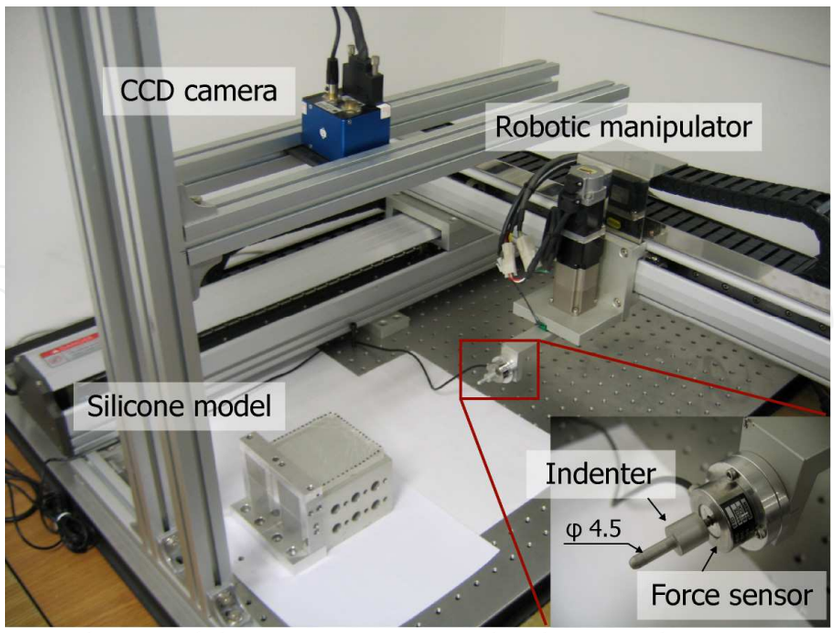

Fig. 5. Experimental setup of slave part in macro-scale telemanipulation system

The geometry of the rectangular-shaped block was represented using 60 control points along the active contour. Hence, the BE model consisted of 60 line elements with 60 nodes. As one side of the block was fixed to the platform, zero displacement boundary conditions were applied on this side. When the indenter deformed the block, the resulting contact force was computed based on the proposed method. Simultaneously, the actual contact force along the indenter insertion axis was measured by the force sensor.

The model prediction was compared with the block response. Fig. 6 shows a comparison between the actual block deformation and the global deformation of the BE model according to dissimilar indentation locations. The dotted line represents the nodes of the BE model; it is determined as a result of the input displacement at the contact point. Each nodal displacement of the BE model is in good agreement with the deformation of the object. The interaction forces at the contact point are shown in Fig. 7. The results show a reasonable match between the actual and estimated force values. While the local strain was raised, the difference between the values was increased due to the linear approximation of the silicone block nonlinearities. A measure of bias (0.0576 N) was also observed due to errors coming from the object buckling along the perpendicular direction to the plane and from measurement errors occurring in the image analysis (e.g., edge detection noise, minor illumination changes). The bias could be overcome using a scaling factor in the case of the micromanipulation system, where the scaled-up reaction force must be reflected to the user.

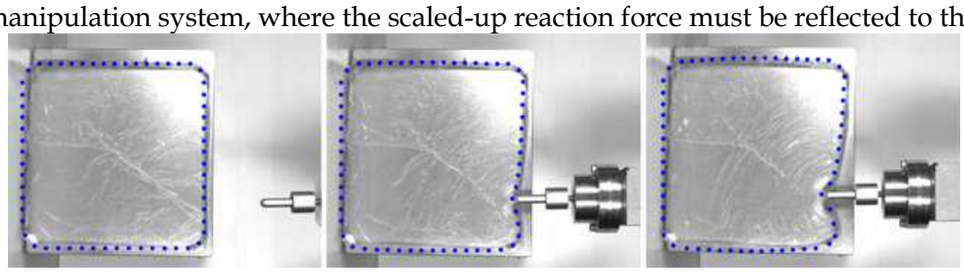

Fig. 6. Deformation of silicone block and BE model (dotted line)

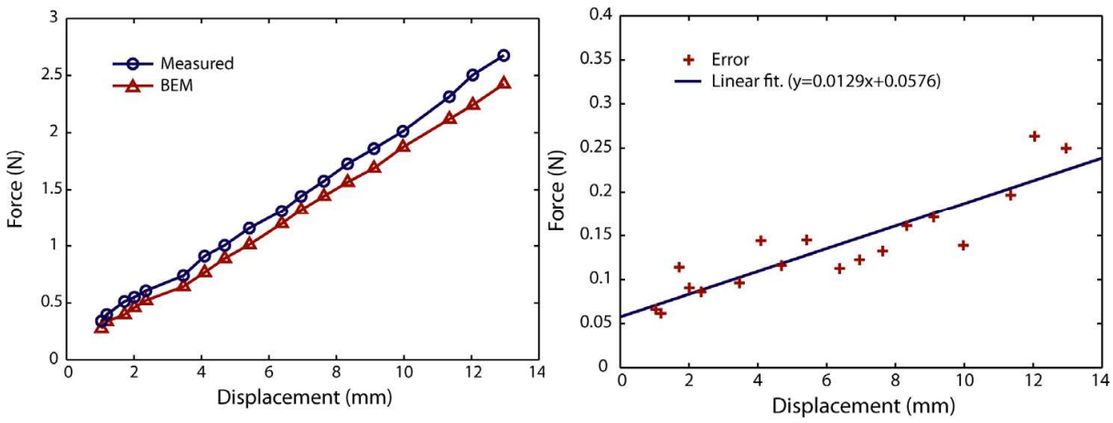

(a) (b)

Fig. 7. (a) Actual surface forces and nodal forces from BEM, and (b) errors along the indentation axis

4.2 Experiment 2: Cellular Manipulation System

In this experiment, an application to cellular manipulation is presented. Cellular manipulations such as a microinjection are now increasingly used in transgenics and in biomedical and pharmaceutical research. Some examples include the creation of transgenic mice by injecting cloned deoxyribonucleic acid (DNA) into fertilized mouse eggs and intracytoplasmic sperm injections (ICSI) with a micropipette. However, most cellular manipulation systems have primarily focused to date on visual information in conjunction with a dial-based console system. The operator needs extensive training to perform these tasks, and even an experienced operator can have low success rates and a poor reproducibility due to the nature of the tasks (Kallio & Kuncova, 2003; Sun & Nelson, 2002).

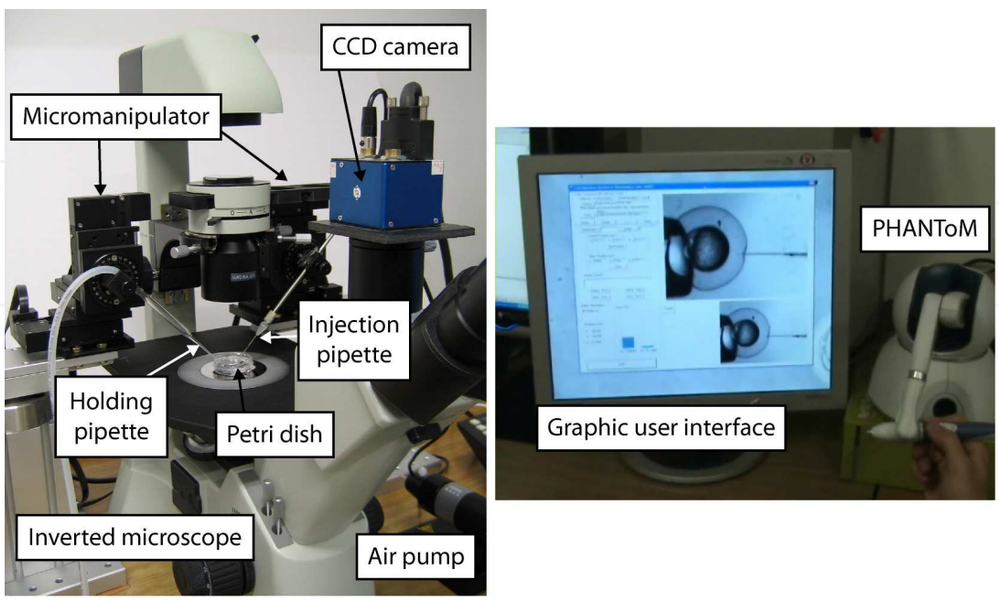

Fig. 8. Developed cellular manipulation system

The developed cell injection system is shown in Fig. 8. It consists of an inverted microscope (Motic, AE31, China) and two 3 DOF micromanipulators (Sutter, MP225, USA) to guide the cell holding and injection units. An injection micropipette (Humagen, MIC-9 μ m-45, USA) is connected to a micromanipulator, whereas a glass capillary with an air pump (Eppendorf, CellTram Air, Germany) is connected to another micromanipulator to hold the cell. Each micromanipulator has a resolution of 0.0625 µm along each axis and a travel distance of 25 mm. Images were captured at a 40× magnification. The obtained images have a size of 640 × 480 pixels and a resolution of 2 µm/pixel.

Zebrafish embryos were used as a deformable object in the experiments. Zebrafish have been widely used as a model in developmental genetic and embryological research due to their similarity to the human gene structure (Stainer, 2001). The embryos are considered as a linear elastic material for research in the small deformation linear theory. It has been reported that the Young's modulus of the chorion of the zebrafish embryo is approximately 1.51 MPa with a standard deviation of 0.07 MPa and that the Poisson's ratio is equal to 0.5 (Kim et al., 2006). These properties were used in the BE model of the cell.

Conventionally, the cell injection procedure involves (i) guiding the injection pipette, (ii) puncturing the membrane, (iii) and depositing the materials. In this work, the task was to puncture the chorion of a zebrafish embryo and to guide the injection pipette to a targeted position. The location of the targeted position was randomly chosen and changed for every test.

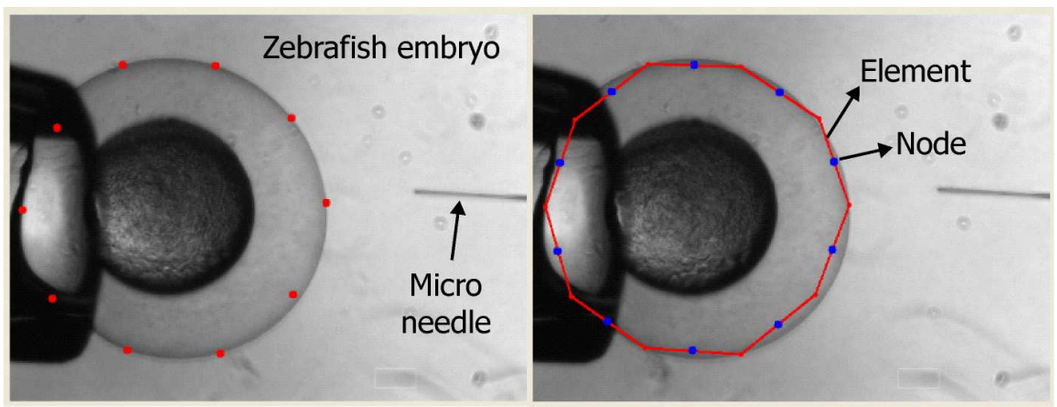

Fig. 9. Edge detection of a zebrafish embryo and BE model with 10 elements.

Fig. 9 shows the edge detection of the zebrafish embryo and the BE model with line elements. The nodes attached to the holding pipette (a glass capillary) have zero displacement boundary conditions..

Unlike macro-scale experiments for the silicone block, and as a result of excessive forces, the cell membrane was punctured in this case using an injection pipette. Therefore, it was necessary to provide the user with a puncturing cue. As the BEM cannot compute the membrane puncturing, the overshoot of the injection pipette after the breaking of the membrane was measured. Published work revealed that the penetration force significantly decreases after puncturing (Kim et al., 2006). Accordingly, when the position overshoot occurred, the magnitude of the reaction force was set to zero.

Fig. 10 shows the estimated force response for the deformation created by the injection pipette. The membrane was punctured when the deformation length ranged approximately between 50 µm and 200 µm. According to previously-published work (Kim et al., 2006), the

force-deformation relationship for a zebrafish embryo is characterized by a nonlinear behavior that can be approximated as linear for small deformations (up to 100 μm). This allows us to use the proposed linear elastic model for small deformations.

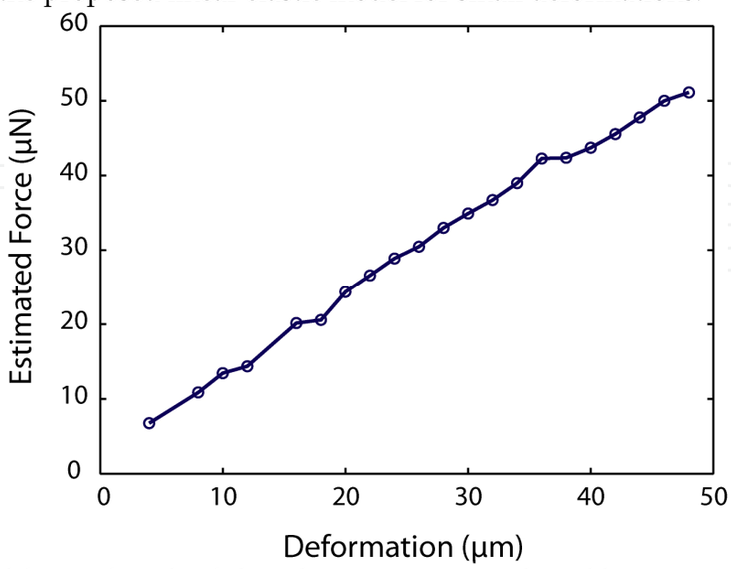

Fig. 10. Estimated force of a zebrafish embryo using vision-based haptic interaction method.

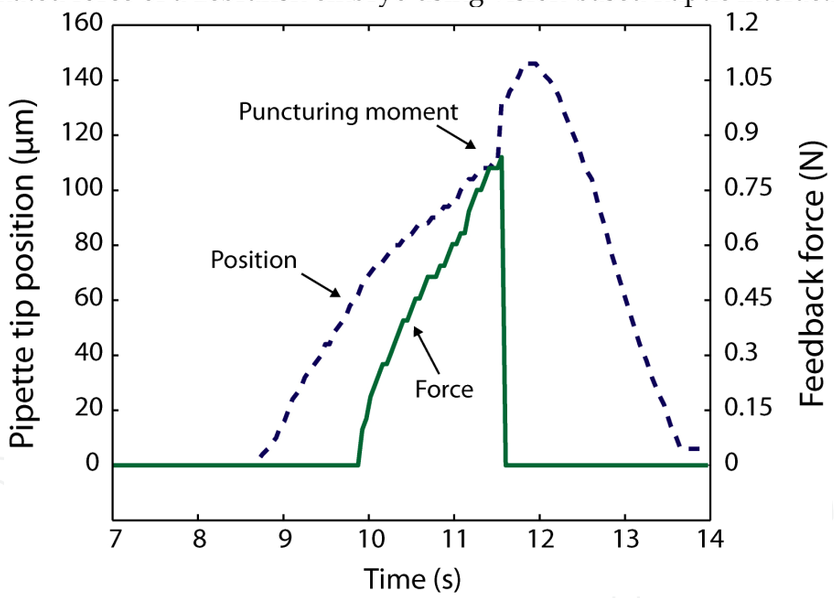

Fig. 11. Amplified cell injection and puncturing force computed using vision-based haptic interaction method

In order to display the force response to a user, the micro contact forces need to be magnified. Specifying and varying the appropriate force scaling factor has been an issue in micromanipulation (Lu et al., 2006; Menciassi et al., 2004). The scaling factor was experimentally chosen within the maximum applicable force of the haptic device (3.3 N). Fig. 11 shows the scaling forces over time for haptic rendering. The forces increase during the insertion of the micropipette, and drop to zero when puncturing occurs.

5. Conclusions and Discussions

In this paper, a haptic rendering algorithm of deformable objects was investigated while inferring the force information of a slave environment using visual information. This method is based on image processing techniques (active contour model and template matching) for the modeling of the slave environment and on a continuum mechanics model for the interactive haptic rendering. Experiments for different scales of telemanipulation systems were performed to demonstrate the effectiveness of the algorithm. The main result is that the developed method can be simply used to estimate the forces without a direct force measurement. The results of two different experiments also showed that the algorithm allows the users to feel reaction forces in real time during the indentation and injection tasks by means of haptic devices.

The advantages of the proposed method over direct force measurements using force sensors can be summarized as follows.

(i) The proposed system only requires a priori knowledge of the object material properties and edge information. These fewer requirements allow the algorithm to be robust to potential topological changes of the model network and do not imply a controlled slave environment.

(ii) The scale of the slave environment does not affect the rendering method. The same algorithm can not only be used in a micro- (or nano-) scale but also in a macro-scale environment. The cellular manipulation system of a zebrafish embryo and the macro-scale telemanipulation experiment of a silicone block showed the potential of the proposed method when applied at different scales. Therefore, it is expected that the developed rendering algorithm can be used in telemanipulation systems with various scales. Examples may include a cellular manipulator, a microassembly system or a telesurgery system. The proposed algorithm is particularly well suited for micromanipulation due to difficulties associated with reliable micro force sensing.

(iii) As the forces are inferred from the object model and the tracked tool tip position, it is not necessary to integrate a force sensor. As a non-contact (indirect) measurement, the developed algorithm will only be slightly affected by breakdowns caused by physical or biochemical interactions. In addition, the visual information of the slave environment is consistently available, as optical devices are installed in the manipulation system.

In the proposed method, the accurate modeling of the deformable objects is a key part for getting a high-fidelity haptic feedback. A number of assumptions and model parameters were required for the physically-based modeling. These could be determined by considering the characteristics of the objects, such as the material properties, geometry and contact conditions. This study assumed that a manipulated object was characterized by linear elastic responses having isotropic and homogeneous properties. However, in reality many deformable objects (e.g., biological cells, soft tissues) are inhomogeneous, anisotropic and made of nonlinear materials. If the aforementioned assumptions enable a rapid computation speed for a better stability of the haptic feedback, the unmodeled behavior might lead to registration problems (modeling error). For example, because the linear elasticity assumption will fail once the model deformation is sufficiently large, the model behavior diverges from that of a deformable object when a large deformation is produced during a manipulation. This modeling error can also be observed due to friction modeling. In our

future work, the detrimental effects of modeling errors on the telemanipulation performance will be studied. If a manipulation task requires a large object deformation or deep interaction, the modeling error in the proposed algorithm might be overcome by adopting a nonlinear modeling approach (Wu et al., 2001) and even an inhomogeneous modeling technique (Jun et al., 2006). The added values will be accompanied by additional computational difficulties introduced by the techniques adopted. An analysis of the trade-off between the added values and the computational burden will also be required.

The BE model was characterized by a priori knowledge of the material properties and geometry obtained from images. The material parameters of many animate and inanimate objects have been measured and determined for various applications including motion analysis, flaw identification and haptic rendering. In this study, the unknown material properties of the deformable objects (the zebrafish embryo and the silicone block) were obtained from literature and using experiments. However, the parameters of other objects of interest may not be readily obtainable. Additional efforts would then be required to objectively determine the physical parameters. In the future work, the authors will strongly consider increasing the available information from the imaging sources. To achieve this goal, an image-based method for the identification of material parameters will be developed by applying an efficient and robust prediction algorithm. The parameters and the interaction forces will be estimated for the input displacements.

At two-dimensional modeling together with a mono image analysis was suitably established in the present experiments in the case of thin planar objects and planar manipulation tasks. An extension of this work to 3D models will be more helpful for many applications. Indeed, a 3D approach will provide additional cues for visual constraints such as those associated with depth information and occlusion.

The developed algorithm has only considered point-contacts between the object and the instrument. However, the measurement of the distribution forces present on the object or the instrument can be achieved using the proposed method without difficulty, while a direct measurement using conventional force sensors is often difficult and sometimes impossible. Another interesting extension will also include the integration of additional haptic feedback modalities, such as a torque feedback.

6. References

Aggarwal, J. K.; Davis, L. S. & Martin, W. N. (1981). Correspondence Processes in Dynamic Scene Analysis. *Proceedings of the IEEE*, Vol. 69, No. 5, 562–572.

Ammi, M.; Ladjal, H. & Ferreira, A. (2006). Evaluation of 3D pseudo-haptic rendering using vision for cell micromanipulation. *Proceedings of IEEE/RSJ International Conference on Intelligent Robots and Systems*, pp. 2115–2120, Beijing, China.

Anis, Y. H.; Mills, J. K. & Cleghorn, W. L. (2006). Vision-based measurement of microassembly forces. *Journal of Micromechanics and Microengineering*, Vol. 16, No. 8, 1639–1652.

Basdogan, C.; De, S., Kim, J., Muniyandi, M., Kim, H. & Srinivasan, M. (2004). Haptics in minimally invasive surgical simulation and training. *IEEE Computer Graphics and Applications*, Vol. 24, No. 2, 56–64.

Chen, E. & Marcus, B. (1998). Force feedback for surgical simulation. *Proceedings of the IEEE*, Vol. 86, No. 3, 524–530.

Delingette, H. (1998). Towards Realistic Soft Tissue Modeling in Medical Simulation. *Proceedings of IEEE: Special Issue on Surgery Simulation*, Vol. 86, No. 3, 512–523.

DiMaio, S. P. & Salcudean, S. E. (2003). Needle insertion modeling and simulation. *IEEE Transactions on Robotics and Automation*, Vol. 19, No. 5, 864–875.

Ferreira, A. & Mavroidis, C. (2006). Virtual reality and haptics for nano robotics: A review study. *IEEE Robotics and Automation Magazine*, Vol. 13, No. 3, 78–92.

Gauthier, M. & Nourine, M. (2007). Capillary Force Disturbances on a Partially Submerged Cylindrical Micromanipulator. *IEEE Transactions on Robotics*, Vol. 23, No. 3, 600–604.

Greminger, M. A. & Nelson, B. J. (2004). Vision-based force measurement. *IEEE Transactions on Pattern Analysis and Machine Intelligence*, Vol. 26, No. 3, 290–298.

Hassanzadeh, I.; Janabi-Sharifi, F., Akhavan, R. & Yang, X. (2005). Teleoperation of mobile robots by shared impedance control: a pilot study. *Proceedings of IEEE International Conference of Control Applications*, pp. 346–351, Toronto, Canada.

Ho, C. H.; Basdogan, C. & Srinivasan, M. A. (1999). Efficient point-based rendering techniques for haptic display of virtual objects. *Presence: Teleoperators and Virtual Environments*, Vol. 8, No. 5, 477–491.

James, D. L. & Pai, D. K. (2003). Multiresolution Green's function methods for interactive simulation of large-scale elastostatic objects. *ACM Transactions on Graphics*, Vol. 22, No. 1, 47–82.

Jun, S.; Choi, J. & Cho, M. (2006). Physics-based s-Adaptive Haptic Simulation for Deformable Object. *Proceedings of 14th Symposium on Haptic Interfaces for Virtual Environment and Teleoperator Systems*, pp. 477–483, Alington, USA.

Kallio, P. & Kuncova, J. (2003). Manipulation of living biological cells: Challenges in automation. *Workshop on microrobotics for biomanipulation in the IROS'03*, Las Vegas, USA.

Kass, M.; Witkin, A. & Terzopoulos, D. (1988). Snakes: active contour models. International *Journal of Computer Vision*, Vol. 1, No. 4, 321–331.

Kennedy, C. W. & Desai, J. P. (2005). A vision-based approach for estimating contact forces: Applications to robot-assisted surgery. *Applied Bionics and Biomechanics*, Vol. 2, No. 1, 53–60.

Kerdok, A. E.; Cotin, S. M., Ottensmeyer, M. P., Galea, A. M., Howe, R. D. & Dawson, S. L., (2003). Truth Cube: Establishing Physical Standards for Soft Tissue Simulation. *Medical Image Analysis*, Vol. 7, No. 3, 283–291.

Kim, D. H.; Hwang, C. N., Sun, Y., Lee, S. H., Kim, B. & Nelson, B. J. (2006). Mechanical analysis of chorion softening in prehatching stages of zebrafish embryos. *IEEE Transactions on Nanobioscience*, Vol. 5, No. 2, 89–94.

Kim, J. S.; Janabi-Sharifi, F. & Kim, J. (2008). A Physically-Based Haptic Rendering for Telemanipulation with Visual Information: Macro and Micro Applications. *Proceeding of the IEEE/RSJ Int. Conf. Intelligent Robots and Systems*, pp. 3489-3494, Nice, France.

Kim, J. S.; Janabi-Sharifi, F. & Kim, J. (2009). Haptic Interaction Method Using Visual Information and Physically-Based Modeling. *IEEE/ASME Trans. Mechatronics*, On review for publication.

Lin, M. & Salisbury, K. (2004). Haptic rendering - Beyond visual computing. *IEEE Computer Graphics and Applications*, Vol. 24, No. 2, 22–23.

Liu, X.; Wang, Y., & Sun, Y. (2007a). Real-time high-accuracy micropipette aspiration for characterizing mechanical properties of biological cells. *Proceedings of IEEE International Conference on Robotics and Automation*, pp. 1930–1935, Rome, Italy.

Liu, X.; Sun, Y., Wang, W., & Lansdorp, B. M. (2007b). Vision-based cellular force measurement using an elastic microfabricated device. *Journal of Micromechanics and Microengineering*, Vol. 17, No. 7, 1281–1288.

Lu, Z.; Chen, P. C. Y. & Lin, W. (2006). Force sensing and control in micromanipulation. *IEEE Transactions on Systems, Man, and Cybernetics, Part C: Applications and Reviews*, Vol. 36, No. 6, 713–724.

Luo, Y. & Nelson, B. J. (2001). Fusing force and vision feedback for manipulating deformable objects. *Journal of Robotic Systems*, Vol. 18, No. 3, 103–117.

Massie, T. H. & Salisbury, J. K. (1994). The PHANToM haptic interface: A device for probing virtual objects. *Proceedings of ASME Dynamic Sys. Control Div.*, pp. 295–301, Chicago, USA.

Mayer, H.; Nagy, I., Knoll, A., Braun, E., Bauernschmitt, R. & Lange, R. (2007). Haptic feedback in a telepresence system for endoscopic heart surgery. *Presence: Teleoperators and Virtual Environments*, Vol. 16, No. 5, 459–470.

Meier, U.; Lopez, O., Monserrat, C., Juan, M. C. & Alcaniz, M. (2005). Real-time deformable models for surgery simulation: a survey. *Computer Methods and Programs in Biomedicine*, Vol. 77, No. 3, 183–197.

Menciassi, A.; Eisinberg, A., Izzo, I. & Dario, P. (2004). From macro to micro manipulation: models and experiments. *IEEE/ASME Trans. Mechatronics*, Vol. 9, No. 2, 311–320.

Metaxas, D. N. & Kakadiaris, I. A. (2002). Elastically Adaptive Deformable Models. *IEEE Transactions on Pattern Analysis and Machined Intelligence*, Vol. 24, No. 10, 1310–1321.

Morris, D.; Neel, J. & Salisbury, K. (2004). Haptic battle pong: High-degree-of-freedom haptics in a multiplayer gaming environment. *Experimental Gameplay Workshop, GDC 2004*, San Jose, USA.

Nelson, B. J.; Sun, Y. & Greminger, M. A. (2005). Microrobotics for molecular biology: Manipulating deformable objects at the microscale. In: *Springer Tracts in Advanced Robotics*, Vol. 15, 115–124, Springer Berlin/Heidelberg.

Ogawa, N.; Oku, H., Hashimoto, K. & Ishikawa, M. (2005). Microrobotic visual control of motile cells using high-speed tracking system. *IEEE Transactions on Robotics*, Vol. 21, No. 4, 704–712.

Owaki, T.; Nakabo, Y., Namiki, A., Ishii, I. & Ishikawa, M. (1999). Real-time system for virtually touching objects in the real world using modality transformation from images to haptic information. *Systems and Computers in Japan*, Vol. 30, No. 9, 17–24.

Salisbury, K.; Brock, D., Massie, T., Swarup, N. & Zilles, C. (1995). Haptic rendering: programming touch interaction with virtual objects. *Proceedings of the 1995 symposium on Interactive 3D graphics*, pp. 123–130, Monterey, California, United States.

Salisbury, K.; Conti, F., & Barbagli, F. (2004). Haptic rendering: introductory concepts. *IEEE Computer Graphics and Applications*, Vol. 24, No. 2, 24–32.

Sitti, M. & Hashimoto, H. (2003). Teleoperated touch feedback from the surfaces at the nanoscale: modeling and experiments. *IEEE/ASME Trans. Mechatronics*, Vol. 8, No. 2, 287–298.

Stainier, D. Y. R. (2001). Zebrafish genetics and vertebrate heart formation. *Nature Reviews Genetics*, Vol. 2, No. 1, 39–48.

Sun, Y. & Nelson, B. J. (2002). Biological cell injection using an autonomous microrobotic system. *International Journal of Robotics Research*, Vol. 21, No. 10-11, 861–868.

Tsap, L. V.; Goldgof, D. B., Sarkar, S. & Powers, P. S. (2000). A method for increasing precision and reliability of elasticity analysis in complicated burn scar cases. *International Journal of Pattern Recognition and Artificial Intelligence*, Vol. 14, No. 2, 189–211.

Wagner, C. R.; Stylopoulos, N., Jackson, P. G. & Howe, R. D. (2007). The Benefit of Force Feedback in Surgery: Examination of Blunt Dissection. *Presence: Teleoperators and Virtual Environments*, Vol. 16, No. 3, 252–262.

Wang, W. H.; Liu, X. Y. & Sun, Y. (2007). Contact detection in microrobotic manipulation. *The International Journal of Robotics Research*, Vol. 26, No. 8, 821–828.

Wang, X.; Ananthasuresh, G. K. & Ostrowski, J. (2001). Vision-based sensing of forces in elastic objects. *Sensors and Actuators A*, Vol. 94, No. 3, 142–156.

Williams, D. J. & Shah, M. (1992). A fast algorithm for active contours and curvature estimation. *CVGIP: Image Understanding*, Vol. 55, No. 1, 14–26.

Wu, X. L.; Downes, M. S., Goktekin, T. & Tendick, F. (2001). Adaptive nonlinear finite elements for deformable body simulation using dynamic progressive meshes. *Computer Graphics Forum*, Vol. 20, No. 3, 349–358.

Zhuang, Y. & Canny, J. (2000). Haptic interaction with global deformations. *Proceedings of IEEE International Conference on Robotics and Automation*, pp. 2428–2433, San Francisco, USA.

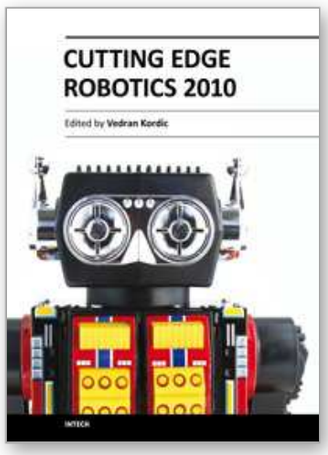

Cutting Edge Robotics 2010

Edited by Vedran Kordic

ISBN 978-953-307-062-9
Hard cover, 440 pages
Publisher InTech
Published online 01, September, 2010
Published in print edition September, 2010

Robotics research, especially mobile robotics is a young field. Its roots include many engineering and scientific disciplines from mechanical, electrical and electronics engineering to computer, cognitive and social sciences. Each of this parent fields is exciting in its own way and has its share in different books. This book is a result of inspirations and contributions from many researchers worldwide. It presents a collection of a wide range of research results in robotics scientific community. We hope you will enjoy reading the book as much as we have enjoyed bringing it together for you.

INTECH
open science | open minds

InTech Europe
University Campus STeP Ri
Slavka Krautzeka 83/A
51000 Rijeka, Croatia
Phone: +385 (51) 770 447
Fax: +385 (51) 686 166
www.intechopen.com

InTech China
Unit 405, Office Block, Hotel Equatorial Shanghai
No.65, Yan An Road (West), Shanghai, 200040, China
中国上海市延安西路65号上海国际贵都大饭店办公楼405单元
Phone: +86-21-62489820
Fax: +86-21-62489821

IntechOpen